well-organized functional sarcomeres. The resultant sarcomere insufficiency (fig. S7) caused both profound baseline contractile deficits and attenuated signaling that limited cardiomyocyte reserve in response to mechanical and adrenergic stress, parameters that are critical to DCM pathogenesis. The consequences of TTN truncation are markedly different from the effects of truncating mutations in another sarcomere protein, myosin-binding protein C (MYBPC); truncation of MYBPC causes enhanced contractile power (18). Our findings also suggest potential therapeutic targets for TTNtvs, including strategies to enhance TTN gene expression, diminish miRNAs that inhibit sarcomerogenesis (15, 19), or stimulate cardiomyocyte signals that improve function (20).

REFERENCES AND NOTES

1. R. E. Hershberger, D. J. Hedges, A. Morales, *Nat. Rev. Cardiol.* **10**, 531–547 (2013).
2. D. S. Herman *et al.*, *N. Engl. J. Med.* **366**, 619–628 (2012).
3. A. M. Roberts *et al.*, *Sci. Transl. Med.* **7**, 270ra6 (2015).
4. Y. H. Loh *et al.*, *Cell Stem Cell* **7**, 15–19 (2010).
5. P. Mali *et al.*, *Science* **339**, 823–826 (2013).
6. T. Boudou *et al.*, *Tissue Eng. Part A* **18**, 910–919 (2012).
7. X. Lian *et al.*, *Nat. Protoc.* **8**, 162–175 (2013).
8. S. Tohyama *et al.*, *Cell Stem Cell* **12**, 127–137 (2013).
9. B. Gerull *et al.*, *Nat. Genet.* **30**, 201–204 (2002).
10. J. L. Tan *et al.*, *Proc. Natl. Acad. Sci. U.S.A.* **100**, 1484–1489 (2003).
11. N. Thavandiran *et al.*, *Proc. Natl. Acad. Sci. U.S.A.* **110**, E4698–E4707 (2013).
12. D. Zhang *et al.*, *Biomaterials* **34**, 5813–5820 (2013).
13. W. A. Linke, *Cardiovasc. Res.* **77**, 637–648 (2008).
14. D. C. Christodoulou, J. M. Gorham, D. S. Herman, J. G. Seidman, *Curr. Protoc. Mol. Biol.* **4**, 4.12 (2011).
15. E. Cai *et al.*, *Stem Cells* **30**, 1746–1755 (2012).
16. J. L. Liu *et al.*, *Life Sci.* **90**, 1020–1026 (2012).
17. S. Ikeda *et al.*, *Mol. Cell. Biol.* **29**, 2193–2204 (2009).
18. F. S. Korte, K. S. McDonald, S. P. Harris, R. L. Moss, *Circ. Res.* **93**, 752–758 (2003).
19. E. van Rooij, E. N. Olson, *Nat. Rev. Drug Discov.* **11**, 860–872 (2012).
20. L. Zentilin *et al.*, *FASEB J.* **24**, 1467–1478 (2010).

SYNTHETIC BIOLOGY

Emergent genetic oscillations in a synthetic microbial consortium

Ye Chen,[1]* Jae Kyoung Kim,[2,3]* Andrew J. Hirning,[1] Krešimir Josić,[4,5] Matthew R. Bennett[1,6]†

A challenge of synthetic biology is the creation of cooperative microbial systems that exhibit population-level behaviors. Such systems use cellular signaling mechanisms to regulate gene expression across multiple cell types. We describe the construction of a synthetic microbial consortium consisting of two distinct cell types—an "activator" strain and a "repressor" strain. These strains produced two orthogonal cell-signaling molecules that regulate gene expression within a synthetic circuit spanning both strains. The two strains generated emergent, population-level oscillations only when cultured together. Certain network topologies of the two-strain circuit were better at maintaining robust oscillations than others. The ability to program population-level dynamics through the genetic engineering of multiple cooperative strains points the way toward engineering complex synthetic tissues and organs with multiple cell types.

Most synthetic gene circuits have been constructed to operate within single, isogenic cellular populations (1–4). However, synthetic microbial consortia could provide a means of engineering population-level phenotypes that are difficult to obtain with single strains (5). Indeed, several synthetic systems have been constructed to exhibit population-level phenotypes (6–9), including synthetic predator-prey systems (10), multicellular computers (11), and spatio-temporal pattern generators (12, 13). We constructed two genetically distinct populations of *Escherichia coli* to create a bacterial consortium that exhibits robust, synchronized transcriptional oscillations that are absent if either strain is grown in isolation. Specifically, we used two different bacterial quorum-sensing systems to construct an "activator" strain and a "repressor" strain that respectively increase and decrease gene expression in both strains. When cultured together in a microfluidic device, the two strains form coupled positive and negative feedback loops at the population level, akin to the circuit topology (i.e., how regulatory components within a circuit regulate each other) of a synthetic dual-feedback oscillator that operates within a single strain (14, 15). We used a combination of mathematical modeling and targeted genetic perturbations to better understand the roles of circuit topology and regulatory promoter strengths in generating and maintaining oscillations. The dual-feedback topology was robust to changes in promoter

strengths and fluctuations in the population ratio of the two strains.

The two synthetic strains in our system were constructed to enzymatically produce and transcriptionally respond to intercellular signaling molecules (Fig. 1A). The activator strain produces C4–homoserine lactone (C4-HSL) (16), a signaling molecule that increases transcription of target genes within the synthetic circuits of both strains. The repressor strain produces 3-OHC14-HSL (17), which decreases transcription in both strains through a synthetic transcriptional inverter (18, 19) mediated by the repressor LacI. These two signaling mechanisms jointly create coupled positive and negative feedback loops at the population level when the two strains are grown together (Fig. 1B). Additionally, each strain, when active, produces the enzyme AiiA, which degrades both signaling molecules, resulting in another layer of negative feedback.

To observe the dynamics of the synthetic consortium, we used a custom-designed microfluidic device in conjunction with time-lapse fluorescence microscopy to observe the two strains as they grew together in a small chamber in which the diffusion time of the HSLs was small (see supplementary materials) (20). Each strain contained a gene encoding a spectrally distinct fluorescent reporter (*cfp*, cyan fluorescent protein, in the activator; *yfp*, yellow fluorescent protein, in the repressor), driven by promoters that respond to both positive and negative signals in the network (Fig. 1A). After an initial transient time, synchronous, in-phase oscillations emerged in the fluorescent reporters of both strains (Fig. 1, C and D). Neither strain oscillated when cultured in isolation (fig. S1). Oscillations had a period of ~2 hours and persisted throughout the experiments (usually more than 14 hours).

The circuit topology of our synthetic consortium consisted of linked positive and negative feedback loops, similar to the topologies of many naturally occurring biological oscillators (21, 22).

[1]Department of Biosciences, Rice University, Houston, TX 77005, USA. [2]Department of Mathematical Sciences, Korea Advanced Institute of Science and Technology, Daejeon 305-701, Korea. [3]Mathematical Biosciences Institute, The Ohio State University, Columbus, OH 43210, USA. [4]Department of Mathematics, University of Houston, Houston, TX 77204, USA. [5]Department of Biology and Biochemistry, University of Houston, Houston, TX 77204, USA. [6]Institute of Biosciences and Bioengineering, Rice University, Houston, TX 77005, USA.
*These authors contributed equally to this work. †Corresponding author. E-mail: matthew.bennett@rice.edu

However, a single negative feedback loop is sufficient to generate rhythms (*14, 23*). Therefore, we tested whether the additional feedback loops in our system were necessary for oscillations. We eliminated either the extra positive or extra negative feedback loop, or both simultaneously. To eliminate the extra positive feedback loop, we created a variant activator strain in which the hybrid promoter $P_{rhl/lac-s}$ was replaced with P_{lac}. We eliminated the additional negative feedback loop by constructing a variant repressor strain without *lacI*. By combining one of the two variant activator strains with one of the two variant repressor strains, we generated consortia with four different topologies (fig. S2): P_2N_2 (containing both additional feedback loops), P_2N_1 (lacking the additional negative feedback loop), P_1N_2 (lacking the additional positive feedback loop), and P_1N_1 (lacking both additional feedback loops). Each topology still contained the negative feedback loop mediated by AiiA.

Each of the topologies described above generated rhythms if and only if both strains were present, confirming that additional feedback loops are not required for oscillations. Further, the oscillations were robust to fluctuations in the population ratio of the two strains in the microfluidic trap (Fig. 2, A to D). In contrast to the effect in a single-strain oscillator (*14*), removing the additional positive feedback loop lengthened the period in P_1N_2 and P_1N_1 (Fig. 2E). Furthermore, P_1N_2 and P_1N_1 generated double-peaked activator oscillations, in contrast to the single-peaked oscillations generated by P_2N_2 and P_2N_1.

To understand the behaviors of the different topologies, we developed a mathematical model (*24, 25*) to simulate the intra- and extracellular dynamics of the key proteins and molecules (see supplementary materials and table S1). In our model, most of the parameters (32 of 40) were either obtained from the literature or by measurement of promoter activity under various conditions (fig. S3 and table S1). The unknown parameters were randomly and independently sampled from uniform distributions covering biologically realistic ranges (see supplementary materials). We obtained 10,000 parameter sets that led to oscillations in four different versions of our model, corresponding to the different network topologies. Of these 10,000 parameter sets, 1506 resulted in rhythms with approximately correct periods (100 to 250 min) for all topologies (fig. S4). More than 40% of these sets gave rise to double-peaked oscillations in the activator strain for both P_1N_2 and P_1N_1, but not P_2N_2 and P_2N_1, matching experimental observations (Fig. 2, C and D, and fig. S5, A to D). In simulations, the periods of P_1N_2 and P_1N_1 were longer when activator oscillations displayed double peaks (Fig. 2F). This indicates that the double peaks and period lengthening of P_1N_2 and P_1N_1 observed in experiments (Fig. 2, C to F) are related. Specifically, the model suggests that both the double peaks and period lengthening of P_1N_2 and P_1N_1 are caused by competition between RhlI and CFP for ClpXP-mediated proteolysis in the activator strain (*26, 27*).
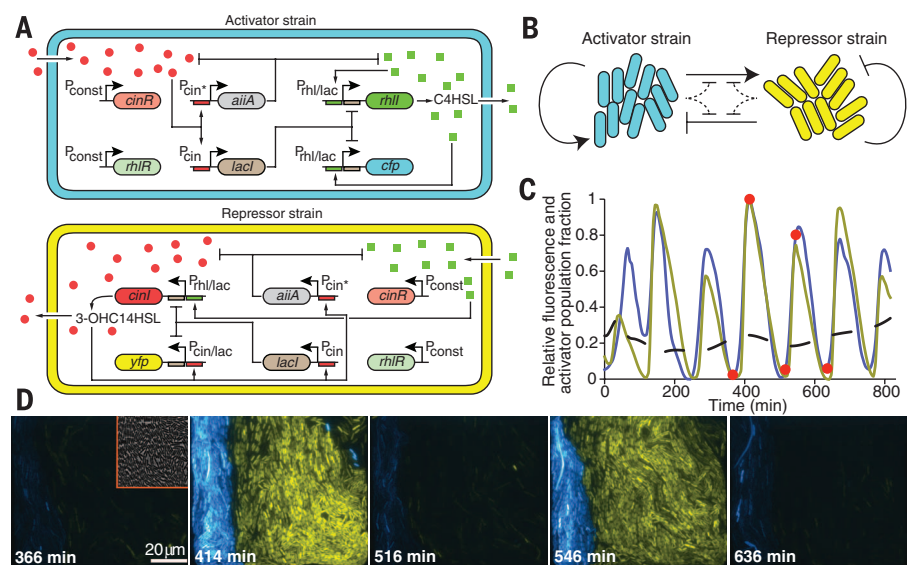

Fig. 1. The synthetic microbial consortium oscillator. (**A**) Circuit diagrams of the activator (top) and repressor (bottom) strains. In the activator strain, transcription of *rhlI* and *cfp* are regulated by separate copies of the hybrid promoter, $P_{rhl/lac}$, which is up-regulated by C4-HSL and down-regulated by LacI. In the repressor strain, *cinI* is driven by the hybrid promoter $P_{rhl/lac}$ and *yfp* is regulated by the hybrid promoter $P_{cin/lac}$, which is up-regulated by 3-OHC14-HSL and down-regulated by LacI. Both strains contain constitutively expressed copies of *cinR* and *rhlR*, which encode transcription factors that respond to the HSLs to regulate their respective promoters, and *aiiA* and *lacI* driven by 3-OHC14-HSL–responsive promoters. (**B**) Global topology of the dual-feedback consortium oscillator. The activator strain up-regulates genes in both strains. The repressor strain down-regulates genes in both strains. AiiA down-regulates signaling (dashed lines, omitted in Figs. 2 and 3 and figs. S2 and S7 for simplicity). (**C**) Representative time series of activator (blue) and repressor fluorescence (yellow), and activator population fraction (black, ratio of the area of activator cells to the area of the entire population of cells, as measured in pixels) for the consortium depicted in (A). Relative fluorescence values are the population average relative to the maximum after background subtraction. (**D**) Five images of the consortium from time points indicated by red dots in (C).
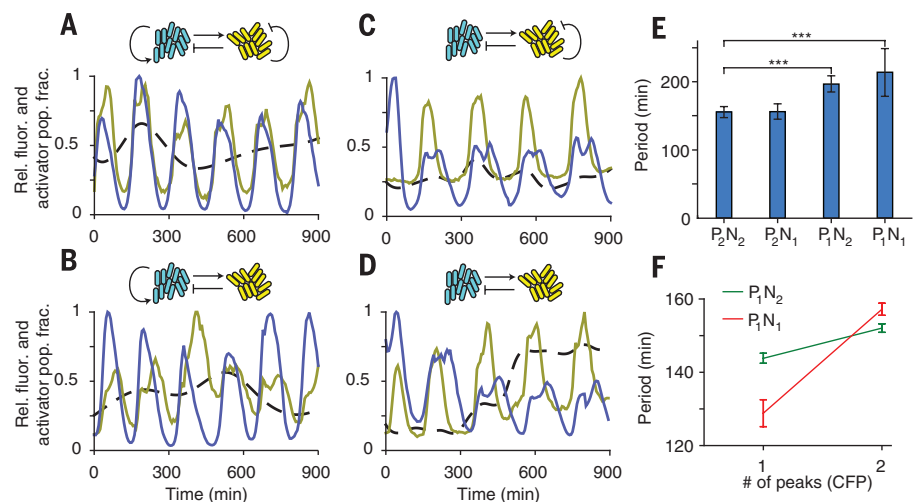

Fig. 2. Dynamics of consortia with various topologies. (**A** to **D**) P_2N_2 (A) and P_2N_1 (B) generate rhythms with shorter periods than P_1N_2 (C) and P_1N_1 (D). The CFP rhythms in the activator strain of P_1N_2 (C) and P_1N_1 (D) exhibited double peaks, in contrast to P_2N_2 (A) and P_2N_1 (B). Here, each line style is the same as in Fig. 1C. (**E**) Experimentally measured periods for each topology. The periods of P_1N_2 ($P < 10^{-11}$) and P_1N_1 ($P < 10^{-6}$) were not the same as that of P_2N_2 (*t* test with Bonferroni correction). Error bars are mean ± SD; from left to right, the number of measured periods was N = 19, 21, 15, 14. (**F**) The mean period (±SEM) of simulated oscillations with parameter sets leading to either single or double peaks in CFP oscillations among the 1506 parameter sets described in the main text. The periods in P_1N_2 and P_1N_1 were longer when CFP oscillations exhibited double peaks.
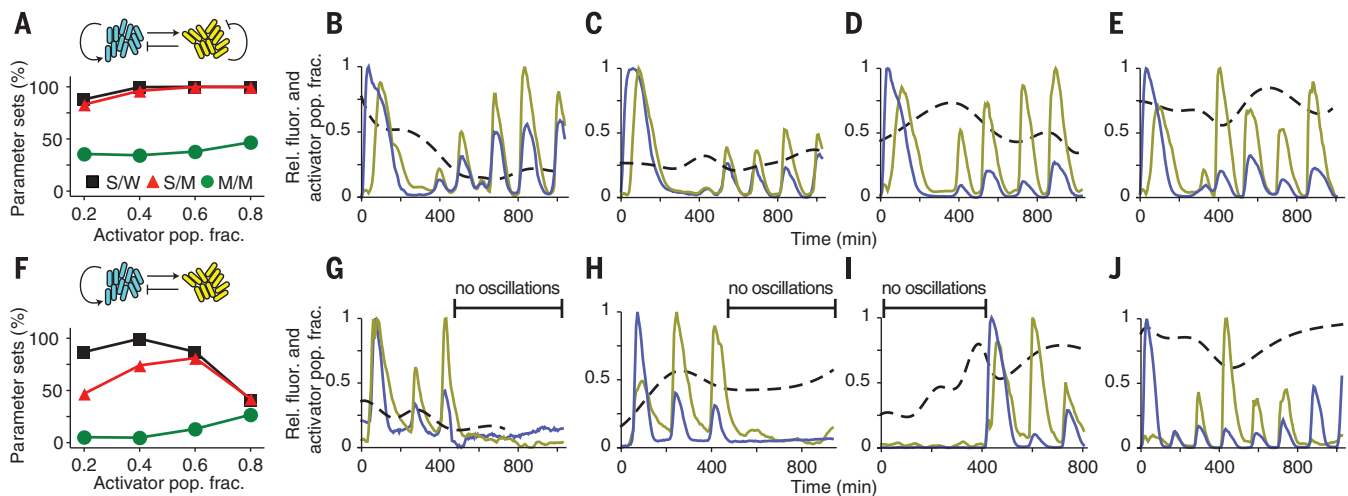
Fig. 3. Additional negative feedback increases robustness. (**A**) Percentage of the 1506 parameter sets (fig. S4) that led to oscillations in the model as a function of percentage of activator strain in the P_2N_2 consortium. Shown are the results for three different combinations of promoter strengths. S/W: $P_{rhl/lac-s}$ and $P_{rhl/lac-w}$ promoters in activator and repressor strains, respectively. S/M: $P_{rhl/lac-s}$ promoter in activator and $P_{rhl/lac-m}$ promoter in repressor. M/M: $P_{rhl/lac-m}$ promoters in both strains. (**B** to **E**) Example trajectories for the P_2N_2 topology with $P_{rhl/lac-m}$ promoters in both activator and repressor strains with different activator population fractions. (**F**) Percentage of the 1506 parameter sets that led to oscillations in the model as a function of percentage of activator strain in the P_2N_1 consortium. Symbols are the same as in (A). Results for P_1N_2 and P_1N_1 are given in fig. S6. (**G** to **J**) Example trajectories for the P_2N_1 topology with the M/M promoter configuration showing occasional loss of oscillations.

We investigated how the additional feedback loops affect the robustness of oscillations, as theoretically additional feedback can increase the robustness of genetic oscillators (*21, 22*). We were interested in two types of perturbations: (i) variations in the population ratio of the two strains, and (ii) different promoter strengths within the circuit. Perturbations in the population ratio of the two strains arose naturally from variations in growth of the two strains within the microfluidic device. To perturb the promoter strengths within the circuits, we altered the $P_{rhl/lac}$ promoters used to drive *cinI* in the repressor strain and *rhlI* in the activator strain to have different expression strengths (see supplementary materials). The original activator strain contained a strong promoter, $P_{rhl/lac-s}$, and the repressor strain a weaker promoter, $P_{rhl/lac-w}$. Gene expression from the strong promoter was approximately 15 times that of the weak promoter. We also created a medium promoter, $P_{rhl/lac-m}$, which was approximately 10 times as strong as the weak promoter (fig. S3).

To examine how changes to the promoter strengths and fluctuations in the population ratio affected oscillations in the mathematical model, we used the 1506 parameter sets described above and systematically altered the parameters governing promoter activities and the population ratio (fig. S3 and table S1). We then calculated the percentage of parameter sets that still led to oscillations in the four different topologies (fig. S6). The mathematical model predicted that P_2N_2 and P_1N_2 show similar robustness (i.e., the percentage of parameter sets leading to oscillations after perturbation was similar) and that both are more robust than P_2N_1 and P_1N_1 (Fig. 3, A and F, and fig. S6). Hence, the model predicts that the addition of a negative feedback loop, but not a positive feedback loop, has a pivotal role in

generating robust rhythms because it tightly regulates repressor concentration (fig. S6) (*22, 28*). Thus, for different promoter-strength combinations, the P_2N_2 oscillator is expected to be more robust to differences in population ratio than P_2N_1 (Fig. 3, A and F). To test this prediction, we constructed P_2N_2 and P_2N_1 using the medium promoter, $P_{rhl/lac-m}$, for both strains. P_2N_2 oscillated over a wide range of population ratios, whereas P_2N_1 occasionally stopped oscillating when the activator population fraction was low (Fig. 3).

We also explored other configurations of promoter strengths within the four topologies. When the promoter driving *cinI* in the repressor strain was changed from $P_{rhl/lac-w}$ to $P_{rhl/lac-m}$ (and $P_{rhl/lac-s}$ was kept in the activator), all topologies still generated oscillations (fig. S7, A to D). However, P_1N_2 and P_1N_1 showed rhythms with a much shorter period than those of P_2N_2 and P_2N_1 (fig. S7, C and D). Furthermore, oscillations in the repressor strain were robust even though activator strain oscillations in P_1N_2 and P_1N_1 were low and unstable.

To understand why the P_1N_2 and P_1N_1 topologies exhibited strong and short-period repressor oscillations even in the absence of strong activator oscillations, we again turned to the mathematical model. Our simulations matched experimental data when $P_{rhl/lac-m}$ was used in the repressor strain in the P_1N_2 and P_1N_1 topologies (fig. S8, A and B). The model predicted that when $P_{rhl/lac-m}$ is used in P_1N_2 and P_1N_1, the mechanism responsible for generating oscillations is an intracellular negative feedback loop mediated by AiiA in the repressor strain and not the intercellular transcriptional negative feedback loop between the two strains (fig. S8). Essentially, the feedback loop mediated by AiiA in the repressor strain has a shorter delay time than the tran-

scriptional loop between the strains, and hence the period becomes shorter (*29*).

Our results show that engineering dynamic population-level phenotypes in synthetic microbial consortia is possible with multiple intercellular signaling mechanisms. Because the population ratio within a consortium can fluctuate, it is important to engineer synthetic circuits that are robust to such perturbations. Overall, our synthetic microbial consortia provide a platform for testing the relation between population-level dynamics and genetic-level regulation.

REFERENCES AND NOTES

1. T. S. Gardner, C. R. Cantor, J. J. Collins, *Nature* **403**, 339–342 (2000).
2. M. B. Elowitz, S. Leibler, *Nature* **403**, 335–338 (2000).
3. A. Levskaya *et al.*, *Nature* **438**, 441–442 (2005).
4. T. Danino, O. Mondragón-Palomino, L. Tsimring, J. Hasty, *Nature* **463**, 326–330 (2010).
5. K. Brenner, L. You, F. H. Arnold, *Trends Biotechnol.* **26**, 483–489 (2008).
6. L. You, R. S. Cox 3rd, R. Weiss, F. H. Arnold, *Nature* **428**, 868–871 (2004).
7. K. Brenner, D. K. Karig, R. Weiss, F. H. Arnold, *Proc. Natl. Acad. Sci. U.S.A.* **104**, 17300–17304 (2007).
8. W. Shou, S. Ram, J. M. G. Vilar, *Proc. Natl. Acad. Sci. U.S.A.* **104**, 1877–1882 (2007).
9. N. Marchand, C. H. Collins, *Biotechnol. Bioeng.* **110**, 3003–3012 (2013).
10. F. K. Balagaddé *et al.*, *Mol. Syst. Biol.* **4**, 187 (2008).
11. A. Tamsir, J. J. Tabor, C. A. Voigt, *Nature* **469**, 212–215 (2011).
12. S. Basu, R. Mehreja, S. Thiberge, M. T. Chen, R. Weiss, *Proc. Natl. Acad. Sci. U.S.A.* **101**, 6355–6360 (2004).
13. S. Basu, Y. Gerchman, C. H. Collins, F. H. Arnold, R. Weiss, *Nature* **434**, 1130–1134 (2005).
14. J. Stricker *et al.*, *Nature* **456**, 516–519 (2008).
15. F. Hussain *et al.*, *Proc. Natl. Acad. Sci. U.S.A.* **111**, 972–977 (2014).
16. E. C. Pesci, J. P. Pearson, P. C. Seed, B. H. Iglewski, *J. Bacteriol.* **179**, 3127–3132 (1997).
17. J. K. Lithgow *et al.*, *Mol. Microbiol.* **37**, 81–97 (2000).
18. Y. Yokobayashi, R. Weiss, F. H. Arnold, *Proc. Natl. Acad. Sci. U.S.A.* **99**, 16587–16591 (2002).

19. J. J. Tabor et al., Cell 137, 1272–1281 (2009).
20. M. R. Bennett, J. Hasty, Nat. Rev. Genet. 10, 628–638 (2009).
21. T. Y. Tsai et al., Science 321, 126–129 (2008).
22. J. K. Kim, D. B. Forger, Mol. Syst. Biol. 8, 630 (2012).
23. B. Novák, J. J. Tyson, Nat. Rev. Mol. Cell Biol. 9, 981–991 (2008).
24. E. L. O'Brien, E. Van Itallie, M. R. Bennett, Math. Biosci. 236, 1–15 (2012).
25. F. Naqib et al., Phys. Rev. E Stat. Nonlin. Soft Matter Phys. 85, 046210 (2012).
26. W. H. Mather, N. A. Cookson, J. Hasty, L. S. Tsimring, R. J. Williams, Biophys. J. 99, 3172–3181 (2010).
27. A. Prindle et al., Nature 508, 387–391 (2014).
28. H. Cho et al., Nature 485, 123–127 (2012).
29. W. Mather, M. R. Bennett, J. Hasty, L. S. Tsimring, Phys. Rev. Lett. 102, 068105 (2009).

MUCOSAL IMMUNOLOGY

The microbiota regulates type 2 immunity through RORγt+ T cells

Caspar Ohnmacht,[1]*† Joo-Hong Park,[1]* Sascha Cording,[1] James B. Wing,[2] Koji Atarashi,[3,4] Yuuki Obata,[5] Valérie Gaboriau-Routhiau,[6,7,8] Rute Marques,[1]‡ Sophie Dulauroy,[1] Maria Fedoseeva,[9] Meinrad Busslinger,[10] Nadine Cerf-Bensussan,[6,7] Ivo G. Boneca,[11,12] David Voehringer,[13] Koji Hase,[5] Kenya Honda,[3,14] Shimon Sakaguchi,[2,15] Gérard Eberl[1]§

Changes to the symbiotic microbiota early in life, or the absence of it, can lead to exacerbated type 2 immunity and allergic inflammations. Although it is unclear how the microbiota regulates type 2 immunity, it is a strong inducer of proinflammatory T helper 17 (T$_H$17) cells and regulatory T cells (T$_{regs}$) in the intestine. Here, we report that microbiota-induced T$_{regs}$ express the nuclear hormone receptor RORγt and differentiate along a pathway that also leads to T$_H$17 cells. In the absence of RORγt+ T$_{regs}$, T$_H$2-driven defense against helminths is more efficient, whereas T$_H$2-associated pathology is exacerbated. Thus, the microbiota regulates type 2 responses through the induction of type 3 RORγt+ T$_{regs}$ and T$_H$17 cells and acts as a key factor in balancing immune responses at mucosal surfaces.

Allergic reactions are on the rise in industrialized nations, paralleling a decrease in the incidence of infectious diseases (1, 2). The hygiene hypothesis proposes that exposure to pathogens reduces the risk of allergy, a notion that may be extended to exposure to the symbiotic microbiota. In support of this hypothesis, germfree mice, devoid of microorganisms, develop increased susceptibility to allergy (3–6). Furthermore, a developmental time window during childhood determines such susceptibility (1, 2). Mice treated early with antibiotics, which deeply affect the microbiota, develop an increased susceptibility to allergy (7) that can last into adulthood (8), an effect also found in mice that remain germfree until weaning (9).

The mechanism by which the microbiota regulates type 2 responses remains unclear. A direct effect of microbiota on type 2 cells, such as T helper 2 (T$_H$) cells and innate lymphoid cells (ILC) 2, has not been documented. In contrast, symbionts are necessary for the differentiation of T$_H$17 cells that produce interleukin (IL)–17 and IL-22 (10), cytokines involved in homeostasis and defense of mucosal surfaces, and a subset of intestinal regulatory T cells (T$_{regs}$) (11). Intriguingly, the absence of extrathymically generated T$_{regs}$ leads to spontaneous type 2 pathologies at mucosal sites (12). As intestinal T$_{regs}$ recognize bacterial antigens (11), the microbiota may regulate type 2 responses through the induction of extrathymically generated T$_{regs}$.

The nuclear hormone receptor RORγt is a key transcription factor for the differentiation of T$_H$17 cells and ILC3s (13, 14). In addition, a substantial fraction of RORγt+ T cells residing in the lamina propria of the small intestine does not express IL-17, but rather IL-10, the T$_{reg}$ marker FoxP3 (a transcription factor), and has regulatory functions (15). Furthermore, the generation of such RORγt+ T$_{regs}$ requires the microbiota (16). Using reporter mice for the expression of RORγt and Foxp3, we found that a majority of RORγt+ T cells in the colon of adult mice expressed Foxp3, and, reciprocally, a majority of colon T$_{regs}$ expressed RORγt (Fig. 1A). The frequency of RORγt+ T$_{regs}$ increased with age, representing most intestinal T$_{regs}$ in 1-year-old mice (fig. S1A). These cells were not found in the thymus (fig. S1B) and did not express Helios or Neuropilin-1, markers of thymically derived T$_{regs}$ (17, 18), in contrast to conventional RORγt– T$_{regs}$ (Fig. 1B and fig. S1C). In the colon, most Helios– T$_{regs}$ were absent in RORγt-deficient mice (Fig. 1B). RORγt+ T$_{regs}$ also expressed an activated CD44^{high} CD62L^{low} phenotype, as well as increased levels of ICOS, CTLA-4, and the nucleotidases CD39 and CD73 (fig. S1C), altogether indicating robust regulatory functions. Another major subset of intestinal T$_{regs}$ expresses Gata3, responds to IL-33, and is involved in the regulation of effector T cells during inflammation (19, 20). Gata3+ T$_{regs}$ were distinct from RORγt+ T$_{regs}$ and expressed Helios, as well as lower levels of IL-10 (fig. S2).

RORγt+ T$_{regs}$ were profoundly reduced in germfree or antibiotic-treated mice, whereas Helios+ and Gata3+ T$_{regs}$ were unaffected (Fig. 1C and fig. S3). Recolonization of germfree mice with a specific pathogen–free (SPF) microbiota restored normal numbers of RORγt+ T$_{regs}$ (fig. S4). Furthermore, a consortium of symbionts composed of 17 Clostridia species efficiently induces the generation of T$_{regs}$ expressing IL-10 in the colon (21), the majority of which expressed RORγt (Fig. 1D). The microbiota has been shown to induce the generation of intestinal T$_{regs}$ through short-chain fatty acids (SCFA) (22, 23) and antigen (11). We found that the SCFA butyrate induced an increase

[1]Institut Pasteur, Microenvironment and Immunity Unit, 75724 Paris, France. [2]Laboratory of Experimental Immunology, Immunology Frontier Research Center, Osaka University, Suita 565-0871, Japan. [3]RIKEN Center for Integrative Medical Sciences (IMS-RCAI), Yokohama, Kanagawa 230-0045, Japan. [4]PRESTO, Japan Science and Technology Agency, Saitama 332-0012, Japan. [5]The Institute of Medical Science, The University of Tokyo, Tokyo 108-8639, Japan. [6]INSERM, U1163, Laboratory of Intestinal Immunity, Paris, France. [7]Université Paris Descartes-Sorbonne Paris Cité and Institut Imagine, Paris, France. [8]INRA Micalis UMR1319, Jouy-en-Josas, France. [9]Center of Allergy and Environment (ZAUM), Technische Universität and Helmholtz Zentrum München, Munich, Germany. [10]Research Institute of Molecular Pathology, Vienna Biocenter, 1030 Vienna, Austria. [11]Institut Pasteur, Biology and Genetics of Bacterial Cell Wall, 75724 Paris, France. [12]INSERM, Groupe Avenir, 75015 Paris, France. [13]Department of Infection Biology at the Institute of Clinical Microbiology, Immunology and Hygiene, University Clinic Erlangen and Friedrich-Alexander University Erlangen-Nuremberg, 91054 Erlangen, Germany. [14]CREST, Japan Science and Technology Agency, 4-1-8 Honcho Kawaguchi, Saitama 332-0012, Japan. [15]Department of Experimental Pathology, Institute for Frontier Medical Sciences, Kyoto University, Kyoto 606-8507, Japan.
*These authors contributed equally to this work. †Present address: Center of Allergy and Environment (ZAUM), Technische Universität and Helmholtz Zentrum München, Munich, Germany. ‡Present address: INSERM, U1163, Laboratory of Intestinal Immunity, and Université Paris Descartes-Sorbonne Paris Cité and Institut Imagine, Paris, France. §Corresponding author. E-mail: gerard.eberl@pasteur.fr